4586 *Inorg. Chem.* **2010**, *49*, 4586–4593
DOI: 10.1021/ic100142u

Inorganic Chemistry
Article

Structural and Magnetic Characteristics of $Gd_5Ga_xSi_{4-x}$

Hui Wang, Sumohan Misra,† Fei Wang, and Gordon J. Miller*

Department of Chemistry and Ames Laboratory, U.S. Department of Energy, Iowa State University, Ames, Iowa 50011. †Current address: SLAC National Accelerator Laboratory, Menlo Park, California 94025

Received January 22, 2010

A crystallographic study and theoretical analysis of the Si/Ga site preferences in the $Gd_5Ga_xSi_{4-x}$ series is presented. $Gd_5Ga_xSi_{4-x}$ adopt the orthorhombic Gd_5Si_4-type structure (space group *Pnma*, $Z = 4$) with a maximum Ga content near $x = 1.00$, as determined by single crystal and powder X-ray diffraction. Refinements from single crystal X-ray diffraction studies of the three independent sites for Si/Ga atoms in the asymmetric unit (interslab T1, intraslab T2 and T3) reveal partial mixing of these elements, with a clear preference for Ga substitution at the interslab T1 sites. To investigate site preferences of Si/Ga atoms, first-principles electronic structure calculations were carried out using the Vienna ab initio simulation package (*VASP*) and the Stuttgart tight-binding, linear-muffin-tin orbital program with the atomic sphere approximation (*TB-LMTO-ASA*). Analysis of various crystal orbital Hamilton population (COHP) curves provide some further insights into the structural tendencies and indicate the roles of both sizes and electronegativities of Ga and Si toward influencing the observed upper limit in Ga content in $Gd_5Ga_xSi_{4-x}$. The magnetic properties of two $Gd_5Ga_xSi_{4-x}$ phases are also reported: both show ferromagnetic behavior with Curie temperatures lower than that for Gd_5Si_4.

Introduction

Since the discovery of a giant magnetocaloric effect (MCE) in $Gd_5Si_2Ge_2$ in 1997, along with other extraordinary magnetic properties such as colossal magnetostriction and giant magnetoresistance,[1−9] a great deal of research has focused on RE_5X_4 systems (RE = rare earth metal; X represents main group elements from groups 13−15) to uncover the mechanism of their extraordinary magneto-responsiveness.[6,7,10] Numerous experimental and theoretical investigations indicate that the giant MCE in $Gd_5Si_2Ge_2$ is associated with a first-order transition,[11,12] during which a structural transition between monoclinic $Gd_5Si_2Ge_2$-type and orthorhombic Gd_5Si_4-type structures accompanies the change in magnetic order. Furthermore, this magnetic-martensitic transition can be controlled by changing chemical composition, temperature, pressure, magnetic field, and valence electron concentration.[12−14]

In an earlier report,[13] we examined the influence of valence electron count on these structure types by replacing tetravalent Ge atoms (metallic radius,[15] $r_m = 1.24$ Å) with size-equivalent, trivalent Ga atoms ($r_m = 1.25$ Å) in Gd_5Ge_4. Gd_5Ge_4 adopts the orthorhombic Sm_5Ge_4-type structure, which is isopointal to the Gd_5Si_4-type and characterized by long (nonbonded) Ge−Ge distances between adjacent $[Gd_5Ge_4]$ slabs. At the upper limit of Ga substitution, that is, $Gd_5Ga_2Ge_2$, these distances dropped to well within covalent bonding lengths so that the structure changes to the Gd_5Si_4-type. Surprisingly, at intermediate compositions, an intermediate orthorhombic structure, Pu_5Rh_4-type $Gd_5Ga_xGe_{4-x}$ was observed. The monoclinic $Gd_5Si_2Ge_2$-type could be observed for $Gd_5Ga_{0.7}Ge_{3.3}$ on cooling below room temperature.[16] Because Ga and Ge cannot be adequately

*To whom correspondence should be addressed. E-mail: gmiller@iastate.edu.

(1) Morellon, L.; Blasco, J.; Algarabel, P. A.; Ibarra, M. R. *Phys. Rev. B* **2000**, *62*, 1022.
(2) Levin, E. M.; Pecharsky, V. K.; Gschneidner, K. A. *Phys. Rev. B* **1999**, *60*, 7993.
(3) Levin, E. M.; Pecharsky, V. K.; Gschneidner, K. A. *Phys. Rev. B* **2001**, *63*, 174110.
(4) Levin, E. M.; Pecharsky, V. K.; Gschneidner, K. A.; Tomlinson, P. *J. Magn. Magn. Mater.* **2000**, *210*, 181.
(5) Magen, C.; Morellon, L.; Algarabel, P. A.; Marquina, C.; Ibarra, M. R. *J. Phys.: Condens. Matter* **2003**, *15*, 2389.
(6) Morellon, L.; Algarabel, P. A.; Ibarra, M. R.; Blasco, J.; Garcia-Landa, B.; Arnold, Z.; Albertini, F. *Phys. Rev. B* **1998**, *58*, R14721.
(7) Morellon, L.; Stankiewicz, J.; Garcia-Landa, B.; Algarabel, P. A.; Ibarra, M. R. *Appl. Phys. Lett.* **1998**, *73*, 3462.
(8) Pecharsky, V. K.; Gschneidner, K. A. *Phys. Rev. Lett.* **1997**, *78*, 4494.
(9) Stankiewicz, J.; Morellon, L.; Algarabel, P. A.; Ibarra, M. R. *Phys. Rev. B* **2000**, *61*, 12651.
(10) Pecharsky, V. K.; Gschneidner, K. A. *Adv. Mater.* **2001**, *13*, 683.
(11) Choe, W.; Miller, G. J.; Meyers, J.; Chumbley, S.; Pecharsky, A. O. *Chem. Mater.* **2003**, *15*, 1413.
(12) Choe, W.; Pecharsky, V. K.; Pecharsky, A. O.; Gschneidner, K. A.; Young, V. G.; Miller, G. J. *Phys. Rev. Lett.* **2000**, *84*, 4617.
(13) Mozharivskyj, Y.; Choe, W.; Pecharsky, A. O.; Miller, G. J. *J. Am. Chem. Soc.* **2003**, *125*, 15183.
(14) Pecharsky, V. K.; Samolyuk, G. D.; Antropov, V. P.; Pecharsky, A. O.; Gschneidner, K. A. *J. Solid State Chem.* **2003**, *171*, 57.
(15) Emsley, J. *The Elements*, 3rd ed.; Clarendon Press: Oxford, 1998;
(16) Misra, S.; Mozharivskyj, Y.; Tsokol, A. O.; Schlagel, D. L.; Lograsso, T. A.; Miller, G. J. *J. Solid State Chem.* **2009**, *182*, 3031.

 Published on Web 04/16/2010

differentiated by X-ray diffraction using Mo K_α radiation because of the one-electron difference in their electron densities, challenges remain to identify clearly how Ga and Ge are distributed throughout the $Gd_5Ga_xGe_{4-x}$ structures. Theoretical assessments of the site preferences by electronic structure calculations suggest Ge atoms are involved in interslab interactions whereas Ga atoms sit within the slabs. Therefore, to address this challenge in part, the $Gd_5Ga_xSi_{4-x}$ series has been synthesized to study their structure−property relationships and to gain further insights about the site preferences between the two main group elements.

Experimental Section

Syntheses. Samples of loaded compositions $Gd_5Ga_xSi_{4-x}$, where $x = 0$, 1.0, 1.5, and 2.0, were prepared by arc-melting about 0.5 g mixtures of the constituent elements under an argon atmosphere on a water-cooled copper hearth. The starting materials were pieces of gadolinium (99.99 wt %, Materials Preparation Center, Ames Laboratory), silicon (99.9999 wt %, Alfa Aesar), and gallium (99.99 wt % Materials Preparation Center, Ames Laboratory). Each arc-melted pellet was turned over and remelted six times to ensure homogeneity; subsequent weight losses during melting were <0.1 wt %. After reaction, every product was broken into halves: one-half was submitted directly for characterization; the other half was sealed in a tantalum tube in an argon atmosphere, then jacketed in evacuated silica tubes, and subsequently annealed at either 900 °C (for $x = 1.5$ and 2.0 samples) or 600 °C (for $x = 1.0$, 1.5, and 2.0 samples) for 24 h. After annealing, the tubes were quenched in cold water. All products are stable toward decomposition after several months storage in air.

Semiquantitative microprobe analyses were performed on several single crystals using a JEOL 5910LV scanning electron microscope equipped with a Noran-Vantage energy-dispersive spectrometer. The chemical compositions obtained from energy dispersive X-ray analysis (EDS) corroborate well with refinements from single crystal data analysis, within the limitation of the technique. No other heavy elements were detected.

Powder X-ray Diffraction. The as-cast and heat-treated samples were examined by room temperature powder X-ray diffraction for phase identification and to assess phase purity. Diffraction patterns were obtained using a Huber 670 Guinier camera with monochromated Cu K_α radiation ($\lambda = 1.54187$ Å). The step size was set at 0.005°, and the exposure time was 1−2 h. Data acquisition was controlled via the in situ program. To explore the purity and homogeneity of all samples, all diffraction patterns were analyzed by Le-Bail refinement using the *LHPM RIETICA* software.[17] Only the scale factor, peak profiles, background, and the lattice parameters of each phase were refined, using Si powder (NIST; $a = 5.430940 \pm 0.000035$ Å) as a calibration standard; these values were in good agreement with the results from single crystal X-ray diffraction.

Single-Crystal X-ray Diffraction. Single-crystal diffraction techniques were used to substantiate powder diffraction results and to refine atomic parameters. Several single crystals from the as-cast samples were mounted on the tips of glass fibers. Room temperature intensity data were collected on a Bruker Smart Apex CCD diffractometer with Mo K_α radiation ($\lambda = 0.71073$ Å) and a detector-to-crystal distance of 5.990 cm. Data were collected over a full sphere of reciprocal space by taking three sets of 606 frames with 0.3° scans in ω and with an exposure time of 10 s per frame. The range of 2θ extended from 4° to 57°. The data were acquired using the *SMART* software.[18] Intensities was extracted and corrected for Lorentz and polarization effects through the *SAINT+* program.[19] Empirical absorption correction was carried out using *SADABS*.[20] Structure solutions and refinements were performed with the *SHELXTL*[21] package of crystallographic programs. Further details of the crystal structure investigations are available from the Fachinformationszentrum Karlsruhe, 76344 Eggenstein-Leopoldshafen, Germany, on quoting the depository number CSD-421365 ($Gd_5Ga_{0.63}Si_{3.38}$), CSD-421366 ($Gd_5Ga_{0.81}Si_{3.18}$), and CSD-421367 ($Gd_5Ga_{0.99}Si_{3.01}$), the name of the authors, and citation of the paper.

Electronic Structure Calculations. To rationalize site preferences for Ga and Si atoms, first-principles electronic structure calculations were carried out using the Vienna ab initio simulation package (*VASP*)[22−25] and the Stuttgart tight-binding, linear-muffin-tin orbital program with the atomic sphere approximation (*TB-LMTO-ASA*).[26] Structural models for these computations were established according to the diffraction results. Total electronic energies of different models of Gd_5GaSi_3 were evaluated as a function of volume using *VASP*. All calculations were performed using projector augmented-wave (PAW) pseudopotentials.[27] A $7 \times 7 \times 7$ Monkhorst−Pack k-points grid was used to sample the first Brillouin zone for reciprocal space integration.[28] The energy cutoff of the plane wave basis was 215 eV. With these settings, the total energy converged to less than 1 meV per unit cell.

TB-LMTO-ASA calculations were carried out to examine the orbital interactions via analysis of densities of states (DOS) and crystal orbital Hamilton population (COHP) curves.[29] For these calculations, the von Barth−Hedin local density approximation[30] was employed for the treatment of exchange and correlation energy. The basis set included Gd 6s, 6p, and 5d orbitals, Si 3s, 3p, and 3d orbitals, and Ga 4s, 4p, and 4d orbitals. The Gd 4f orbitals were treated as half-filled core wave functions. Also, the Si 3d and Ga 4d orbitals were treated by the Löwdin downfolding technique.[31] The Wigner−Seitz radii of the atomic spheres were 1.87−2.06 Å for Gd, 1.48−1.53 Å for Si, and 1.53 Å for Ga, which filled the unit cell with about 8.6% overlap without introducing any empty spheres. A total of 256 ($8 \times 4 \times 8$) k-points in the irreducible wedge of the orthorhombic first Brillouin zone were used for integration.

Magnetic Property Measurements. Magnetic measurements were performed using a Quantum Design, Inc. MPMS XL-7 SQUID magnetometer on as-cast polycrystalline samples in the temperature interval 1.7−400 K and in magnetic fields up to 70 kOe. Only samples that gave single-phase powder X-ray diffraction patterns, that is, samples refined as $Gd_5Ga_{0.63}Si_{3.37}$ and $Gd_5Ga_{0.81}Si_{3.19}$, were used for these measurements. Experiments included direct current (dc) magnetic susceptibility measurements between about 2 and 400 K and isothermal magnetization measurements in dc magnetic fields varying up to 50 kOe. For the susceptibility measurements, the samples were first cooled under zero magnetic field (zfc) and then the susceptibilities were measured on heating under a 1 kOe magnetic field. The measurements were then repeated upon cooling with the magnetic field turned on (fc). All data were fit to a modified Curie−Weiss Law in the corresponding paramagnetic regions. Curie temperatures were determined as a maximum on dM/dT

(17) Hunter, B. A.; Howard, C. J. *LHPM-Rietica*, 1.71; Australian Nuclear Science and Technology Organization: Menai, Australia, 2000.
(18) *SMART*, 5.625; Bruker AXS Inc.: Madison, WI, 2001.
(19) *SAINT+*, 6.22; Bruker AXS Inc.: Madison, WI, 2001.
(20) *SADABS*, 2.03; Bruker AXS Inc.: Madison, WI, 2001.
(21) *SHELXTL*, 6.10; Bruker AXS Inc.: Madison, WI, 2000.
(22) Kresse, G.; Furthmuller, J. *Comput. Mater. Sci.* **1996**, *6*, 15.
(23) Kresse, G.; Furthmuller, J. *Phys. Rev. B* **1996**, *54*, 11169.
(24) Kresse, G.; Hafner, J. *Phys. Rev. B* **1993**, *47*, 558.
(25) Kresse, G.; Hafner, J. *Phys. Rev. B* **1994**, *49*, 14251.
(26) Jepsen, O.; Andersen, O. K. *TB-LMTO*, 47; MPI-FKF: Stuttgart, Germany, 2000.
(27) Kresse, G.; Joubert, D. *Phys. Rev. B* **1999**, *59*, 1758.
(28) Monkhorst, H. J.; Pack, J. D. *Phys. Rev. B* **1976**, *13*, 5188.
(29) Dronskowski, R.; Blochl, P. E. *J. Phys. Chem.* **1993**, *97*, 8617.
(30) Barth, U. V.; Hedin, L. *J. Phys. C: Solid State Phys.* **1972**, *5*, 1629.
(31) Lambrecht, W. R. L.; Andersen, O. K. *Phys. Rev. B* **1986**, *34*, 2439.

Table 1. Lattice Parameters for As-Cast and Annealed (600 °C; Italics) $Gd_5Ga_xSi_{4-x}$ (x(Loaded) = 0, 1.0, 1.5, 2.0) Samples[a]

x(Loaded)	a (Å)	b (Å)	c (Å)	V (Å^3)
0	7.485(1)	14.739(1)	7.743(1)	854.2(1)
1.0	7.485(5) *7.483(3)*	14.831(6) *14.835(5)*	7.801(4) *7.811(3)*	866.1(5) *867.1(1)*
1.5	7.477(2) *7.480(2)*	14.835(4) *14.850(7)*	7.821(4) *7.823(4)*	867.6(4) *869.0(4)*
2.0	7.482(4) *7.486(3)*	14.869(2) *14.883(2)*	7.838(9) *7.837(9)*	871.9(9) *873.2(6)*

[a]As obtained by powder X-ray Diffraction: Gd_5Si_4-type, space group *Pnma* (No. 62), Cu Kα radiation, 2θ range = 4−100°, T = 298 K, Z = 4.

curves. All data were corrected for temperature independent contributions, that is, $\chi_{measured} = \chi_{TIP} + C/(T-\Theta_p)$.

Results and Discussion

Synthesis and Structural Features. The powder X-ray diffraction patterns of all as-cast $Gd_5Ga_xSi_{4-x}$ (x = 0, 1.0, 1.5, 2.0) samples contained a phase that could be indexed by the orthorhombic Gd_5Si_4-type structure, space group *Pnma*. The refined lattice parameters obtained from powder X-ray diffraction are listed in Table 1. The as-cast samples loaded with x = 1.0 and 1.5 contained the Gd_5Si_4-type phase as the dominant phase; the as-cast sample $Gd_5Ga_2Si_2$ (x = 2.0) contained significant amounts Gd_3Ga_2 and GdGa as secondary phases (Gd_3Ga_2: ca. 20%, GdGa: ca. 15%). After annealing $Gd_5Ga_xSi_{4-x}$ (x = 1.5, 2.0) at 900 °C for 24 h, the $Gd_5Ga_2Si_2$ sample decomposed completely to Gd_5Ga_3 (Mn_5Si_3-type, ca. 25%), GdGa (ca. 30%) and Gd_3Ga_2 (ca. 45%), but $Gd_5Ga_{1.5}Si_{2.5}$ still contained about one-half of the primary Gd_5Si_4-type phase in addition to the secondary phases Gd_5Ga_3 (ca. 25%) and GdGa (ca. 20%), which presumably formed upon decomposition of the main phase. Annealing the ternary samples $Gd_5Ga_xSi_{4-x}$ (x = 1.0, 1.5, 2.0) at 600 °C for 24 h improves sample crystallinity, as seen by narrower diffraction peaks, but also increases the amount of secondary phases (see Figure 1). The Mn_5Si_3-type phases grow in especially as seen by reflections between 40 and 45° (these reflections are the most intense based on a theoretically calculated pattern); the GdGa-type phase also grows significantly, but its most intense reflections overlap reflections of $Gd_5Ga_xSi_{4-x}$ in the region 30−35°. Table 1 includes refined lattice constants of the Gd_5Si_4-type phases after annealing in comparison to the as-cast products. Although some peaks slightly shift their scattering angles after annealing, there are no statistically significant changes in lattice parameters or unit cell volumes.

Single-crystal diffraction was used to refine atomic parameters in these phases. The crystallographic data, atomic positions, site occupancies, and isotropic displacement parameters obtained from single crystal X-ray diffraction from specimens extracted from each product are listed in Tables 2 and 3. There is good agreement between unit cell parameters obtained by powder and single-crystal X-ray diffraction. The orthorhombic crystal structure consists of about 7.4 Å thick slabs with composition [$Gd_5(Ga_xSi_{4-x})$], and has six atoms in the asymmetric unit: three different sites for Gd atoms and three different sites for Si or Ga atoms, sites which are labeled as T1 for atoms involved in interslab bonding and T2, T3 for those involved in intraslab bonds (see Figure 2). Refinement of the occupancies at the T1, T2, and T3 sites reveals clear preference for Ga atoms at the T1 sites and for Si atoms at the T2 and T3 sites. Naturally,

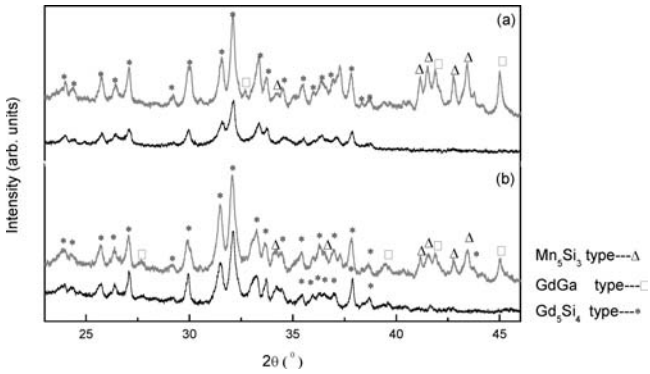

Figure 1. Schematic representation of powder X-ray diffraction patterns of the as-cast and heat-treated samples of loaded compositions $Gd_5Ga_xSi_{4-x}$ (a) x = 1.0 and (b) x = 1.5. The black line represents the as-cast samples; the gray line is for the heat-treated samples. Peaks unambiguously originating from impurity phases attributed to Mn_5Si_3- and GdGa-type structures are also marked.

as the Ga concentration increases, all the occupancies of Ga also increase (Figure 3). Furthermore, the refined chemical compositions give lower Ga contents than the loaded composition; the maximum refined composition is $Gd_5Ga_{0.99(4)}Si_{3.01}$. These two results differ from our earlier work on the $Gd_5Ga_xGe_{4-x}$,[13] in which the maximum Ga composition was reported to be $Gd_5Ga_2Ge_2$, and Ga atoms preferred the T2 and T3 sites (according to theoretical calculations because Ga and Ge could not be unequivocally differentiated by conventional X-ray diffraction techniques).

Significant interatomic distances for Gd_5Si_4 and $Gd_5Ga_{0.99(4)}Si_{3.01}$ are summarized in Table 4 (results for the other crystals are included in the Supporting Information). As expected, most interatomic distances and the unit cell volumes in $Gd_5Ga_xSi_{4-x}$ increase as the Ga content increases. However, there are a few notable trends: (i) the *a*-axis lengths remain constant with Ga content, whereas the *b*- and *c*-axis lengths increase monotonically with Ga content; (ii) both T1−T1 and T2−T3 distances increase with increasing Ga concentration, with the T1−T1 increasing at a greater rate; and (iii) interatomic distances within slabs generally increase with increasing Ga content, but a single T1−Gd1 distance, which is an *interslab* contact, drops sharply. All three structural observations are influenced by both size and electronic effects from substituting Ga for Si. The unusual trend in *a*-axis length resembles the effect in $Gd_5Ga_xGe_{4-x}$,[13] which shows a clear decrease in this parameter with increasing Ga content. In $Gd_5Ga_xSi_{4-x}$, *a*-axis changes due to the counteracting forces of increasing size (Ga vs Si) and decreasing valence electron count (see subsequent section) are effectively eliminated. The different behavior observed for the T1−T1 and T2−T3 distances is consistent with the systematically larger

Table 2. Crystallographic Data for $Gd_5Ga_xSi_{4-x}$ (x = 0, 1, 1.5, 2)[a]

	0	1	1.5	2.0
loaded comp.	Gd_5Si_4	Gd_5GaSi_3	$Gd_5Ga_{1.5}Si_{2.5}$	$Gd_5Ga_2Si_2$
refined comp.	Gd_5Si_4	$Gd_5Ga_{0.63(2)}Si_{3.37}$	$Gd_5Ga_{0.81(3)}Si_{3.18}$	$Gd_5Ga_{0.99(4)}Si_{3.01}$
a (Å)	7.478(2)	7.485(1)	7.481(1)	7.481(2)
b (Å)	14.723(4)	14.833(2)	14.863(2)	14.884(3)
c (Å)	7.743(2)	7.809(1)	7.825(1)	7.835(2)
volume (Å^3)	852.5(4)	866.9(2)	870.0(2)	872.5(3)
ind. refl.	1073	1083	1079	1084
no. parameters	46	49	49	49
final R indices [$I > 2\sigma(I)$]	R1 = 0.0364, wR2 = 0.0659	R1 = 0.0233, wR2 = 0.0491	R1 = 0.0306, wR2 = 0.0537	R1 = 0.0365, wR2 = 0.0608
peak/hole (e$^-$/Å^3)	2.808/−2.200	2.258/−1.272	2.044/−1.749	2.631/−1.831

[a]As obtained by single crystal X-ray diffraction: Space group *Pnma* (No. 62), Mo Kα radiation, 2θ range = 4−57°, T = 298 K, Z = 4.

Table 3. Atomic Coordinates (×10^4), Site Occupancies, and Isotropic Displacement Parameters (Å^2; ×10^3) for $Gd_5Ga_xSi_{4-x}$ As Obtained by Single Crystal X-ray Diffraction[a]

Atom		x	y	z	SOF	U_{eq}
			Gd_5Si_4			
Gd1	8*d*	289(1)	5972(1)	1821(1)	1	12(1)
Gd2	8*d*	3160(1)	1223(1)	1797(1)	1	11(1)
Gd3	4*c*	1441(1)	2500	5110(1)	1	11(1)
Si1	8*d*	1436(4)	406(2)	4733(4)	1	12(1)
Si2	4*c*	204(6)	2500	999(6)	1	13(1)
Si3	4*c*	2582(6)	2500	8769(6)	1	12(1)
			$Gd_5Ga_{0.63(2)}Si_{3.37}$			
Gd(1)	8*d*	253(1)	5962(1)	1821(1)	1	12(1)
Gd(2)	8*d*	3183(1)	1225(1)	1790(1)	1	11(1)
Gd(3)	4*c*	1484(1)	2500	5135(1)	1	12(1)
T(1)	8*d*	1491(2)	400(1)	4713(2)	0.18(1)	13(1)
T(2)	4*c*	231(3)	2500	1005(3)	0.11(1)	12(1)
T(3)	4*c*	2619(3)	2500	8760(3)	0.15(1)	12(1)
			$Gd_5Ga_{0.81(3)}Si_{3.18}$			
Gd(1)	8*d*	243(1)	5958(1)	1817(1)	1	13(1)
Gd(2)	8*d*	3188(1)	1224(1)	1787(1)	1	11(1)
Gd(3)	4*c*	1499(1)	2500	5146(1)	1	13(1)
T(1)	8*d*	1506(3)	402(1)	4713(3)	0.23(1)	11(1)
T(2)	4*c*	241(4)	2500	1012(4)	0.17(1)	14(1)
T(3)	4*c*	2626(4)	2500	8757(4)	0.19(1)	12(1)
			$Gd_5Ga_{0.99(4)}Si_{3.01}$			
Gd(1)	8*d*	237(1)	5955(1)	1815(1)	1	14(1)
Gd(2)	8*d*	3190(1)	1225(1)	1786(1)	1	12(1)
Gd(3)	4*c*	1504(1)	2500	5150(1)	1	14(1)
T(1)	8*d*	1513(3)	399(2)	4708(3)	0.29(1)	15(1)
T(2)	4*c*	232(5)	2500	1009(5)	0.19(1)	13(1)
T(3)	4*c*	2627(5)	2500	8763(4)	0.22(1)	13(1)

[a]All T1, T2, and T3 sites are fully occupied with a mixture of Ga and Si atoms; only Ga occupations are listed. The only exception is Gd_5Si_4, where the T1, T2, and T3 sites are fully occupied by Si atom.

occupation of Ga at the T1 site than in either the T2 or the T3 sites. Finally, the dramatic decrease in an interslab T1−Gd1 distance correlates with the increasing T1−T1 distance, and is observed as structures with the Gd_5Si_4-type structure transform into the Pu_5Rh_4-type or Sm_5Ge_4-type structures.[13,16]

Computational Models and the Coloring Problem. Distribution of different elements over various independent sites in a structure is known as a coloring problem.[32] Although electronic and geometric factors often dictate atomic separation, the entropy contribution to the Gibbs free energy always favors a statistical mixture.[33,34] Nevertheless, in as-cast $Gd_5Ga_xSi_{4-x}$ structures, there is a clear preference for Ga atoms in the T1 sites, which implies a significant enthalpic contribution to the distribution. To investigate the distribution of Ga atoms among the T1, T2, and T3 sites, we constructed five different unit cells as computational models for "Gd_5GaSi_3" according to the

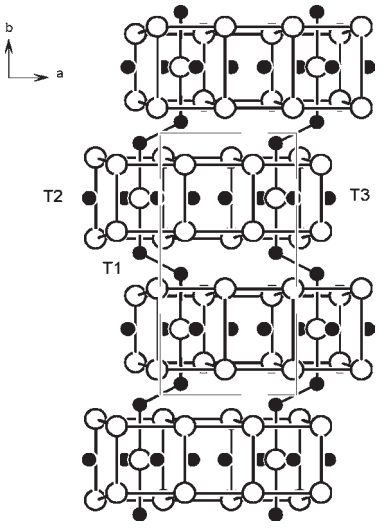

Figure 2. Crystal structure of $Gd_5Ga_xSi_{4-x}$ (Gd_5Si_4-type) projected along the c-axis.

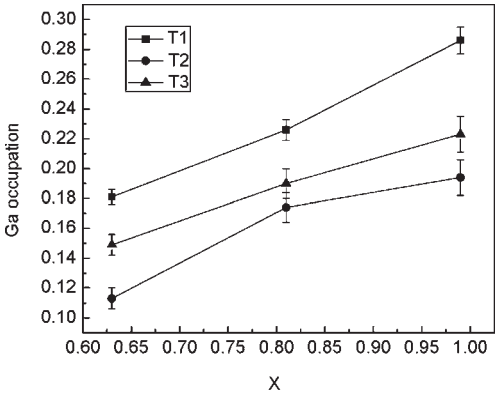

Figure 3. Refined Ga occupation in each T site in $Gd_5Ga_xSi_{4-x}$ as a function of total Ga concentration.

(32) Miller, G. J. *Eur. J. Inorg. Chem.* **1998**, *5*, 523.

(33) Mozharivskyj, Y.; Kaczorowski, D.; Franzen, H. F. *J. Solid State Chem.* **2000**, *155*, 259.

(34) Mozharivskyj, Y.; Franzen, H. F. *J. Alloys Compd.* **2001**, *319*, 100.

Table 4. Selected Interatomic Distances for the Two Limiting Cases, Gd_5Si_4 and $Gd_5Ga_{0.99(4)}Si_{3.01}$[a]

atom pairs	Gd_5Si_4 (Å)	$Gd_5Ga_{0.99(4)}Si_{3.01}$ (Å)	atom pairs	Gd_5Si_4 (Å)	$Gd_5Ga_{0.99(4)}Si_{3.01}$ (Å)
T1-T1(×4)	2.493(6)	2.597(5)	T3-Gd1(×8)	3.142(3)	3.176(3)
			Gd1(×8)	3.143(3)	3.189(3)
T2-T3(×4)	2.479(7)	2.511(5)	Gd2(×8)	3.036(4)	3.065(3)
			Gd3(×4)	2.959(5)	2.953(4)
T1-Gd1(×8)	3.051(3)	3.054(3)	Gd3(×4)	3.014(5)	3.023(4)
Gd1(×8)	3.078(3)	3.134(2)			
Gd2(×8)	2.877(3)	2.885(2)	Gd1−Gd1(×8)	3.884(1)	3.891(1)
Gd2(×8)	2.975(3)	3.009(3)	Gd2(×8)	3.826(1)	3.834(1)
Gd1(×8)	3.152(3)	3.179(3)	Gd2(×8)	4.041(1)	4.088(1)
Gd1(×8)	3.723(2)	3.640(1)	Gd2(×8)	4.076(1)	4.132(1)
Gd2(×8)	2.898(3)	2.923(3)	Gd3(×8)	3.519(1)	3.555(1)
Gd3(×8)	3.097(3)	3.146(3)	Gd3(×8)	3.578(1)	3.597(1)
			Gd1(×4)	4.041(1)	4.037(2)
T2-Gd1(×8)	3.157(4)	3.211(3)	**Gd2(×8)**	3.758(1)	3.750(1)
Gd2(×8)	2.964(4)	2.979(3)	**Gd2(×8)**	3.880(1)	3.925(1)
Gd2(×8)	2.967(4)	2.987(3)			
Gd3(×4)	2.941(5)	2.934(4)	Gd2−Gd2(×4)	3.761(2)	3.797(2)
Gd3(×4)	3.314(5)	3.381(4)	Gd2(×8)	3.894(2)	3.904(1)
			Gd3(×8)	3.426(1)	3.471(2)
			Gd3(×8)	3.430(1)	3.485(1)

[a] The entries in bold within the T1-Gd# and Gd1−Gd# distances separate intraslab (not bold) from interslab (bold) contacts (see Figure 2 for illustration of the structure with respect to slabs). A complete listing of interatomic distances is available in the Supporting Information.

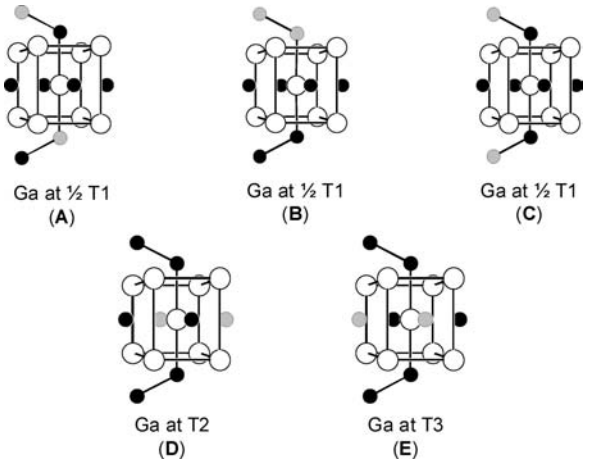

Figure 4. Coordination environments of the Gd3 atoms in the five computational models of Gd_5GaSi_3. The light gray circles are Ga atoms; black circles are Si atoms; white circles are Gd atoms. Occupation of Ga atoms at the T1, T2, or T3 sites is noted.

results obtained from the refinements of powder and single-crystal X-ray diffraction. Fragments of these models surrounding the Gd3 (4*c*) sites are illustrated in Figure 4. Three of these models, (**A**), (**B**), and (**C**), involve breaking the equivalence of the T1 (8*d*) sites in space group *Pnma* by placing 4 Ga and 4 Si atoms among these 8 positions in the unit cell. Models (**A**) and (**C**) contain just Ga−Si (T1−T1) contacts, whereas (**B**) has Ga−Ga and Si−Si contacts. (**A**) and (**C**) differ by the environments created at the Gd3 (4*c*) sites: in (**A**), all Gd3 sites are equivalent; in (**C**), there are two distinct Gd3 sites. Finally, models (**D**) and (**E**) retain the space group *Pnma* of the Gd_5Si_4-type structure with Ga placed, respectively, at the T2 and T3 sites. Both of these models involve just intraslab Ga−Si (T2−T3) contacts.

To set up a computational model for chemical bonding analysis of Gd_5GaSi_3 via densities of states (DOS) and crystal orbital Hamilton population (COHP) curves, we first determined the coloring scheme of Ga and Si atoms,

Table 5. Total Energies[a] and Space Groups by *VASP* Calculations for Gd_5GaSi_3

	type				
	(**A**)	(**B**)	(**C**)	(**D**)	(**E**)
space group	$Pn2_1a$	$P2_1/c$	$P2_1ma$	*Pnma*	*Pnma*
E (meV/f.u.)	0	69.9	2.2	115.8	88.0
E (K/f.u.)	0	811	26	1344	1021

[a] Relative to the minimum energy structure (**A**).

a scheme which gives the lowest total energy and would be the most desirable model to compare with the experimental results. To identify this coloring scheme, first principles calculations using the *VASP* code were carried out on the five models described above (see also Figure 4). The calculated total energies per formula unit are listed in Table 5 and indicate that models (**A**) and (**C**) are the energetically preferred arrangements of Ga atoms for Gd_5GaSi_3. These results clearly indicate that it is most favorable for the Ga atoms to occupy the T1 sites, a result which is consistent with the refined site occupancies obtained from single-crystal diffraction results. Moreover, among the three possibilities for Ga substitution at the T1 sites, Ga−Si contacts are more energetically favorable than Ga−Ga/Si−Si bonds. Furthermore, the slight preference for Ga atoms in the T3 sites over the T2 sites is also suggested by the relative total energies. For further chemical bonding analysis, Model (**A**) was chosen to represent the experimental structure although this model neglects effects due to statistical mixing.

We can use the results in Table 5 to predict the distributions of Ga atoms among the T1, T2, and T3 sites semiquantitatively, by using the configurational entropy based on a Boltzmann distribution of these five model structures. At 1000 K, the statistical distribution of Ga atoms is predicted to be 39.8% at T1, 8.6% at T2, and 11.9% at T3; at 3000 K, the corresponding distribution would be 33.5% Ga at T1, 15.6% Ga at T2, and 17.3% Ga at T3. The experimental result for $Gd_5Ga_{0.99(4)}Si_{3.01}$ refined as 29(1)% Ga at T1, 19(1)% Ga at T2, and 22(1)% Ga at T3. At this point, we attempted refinements of the

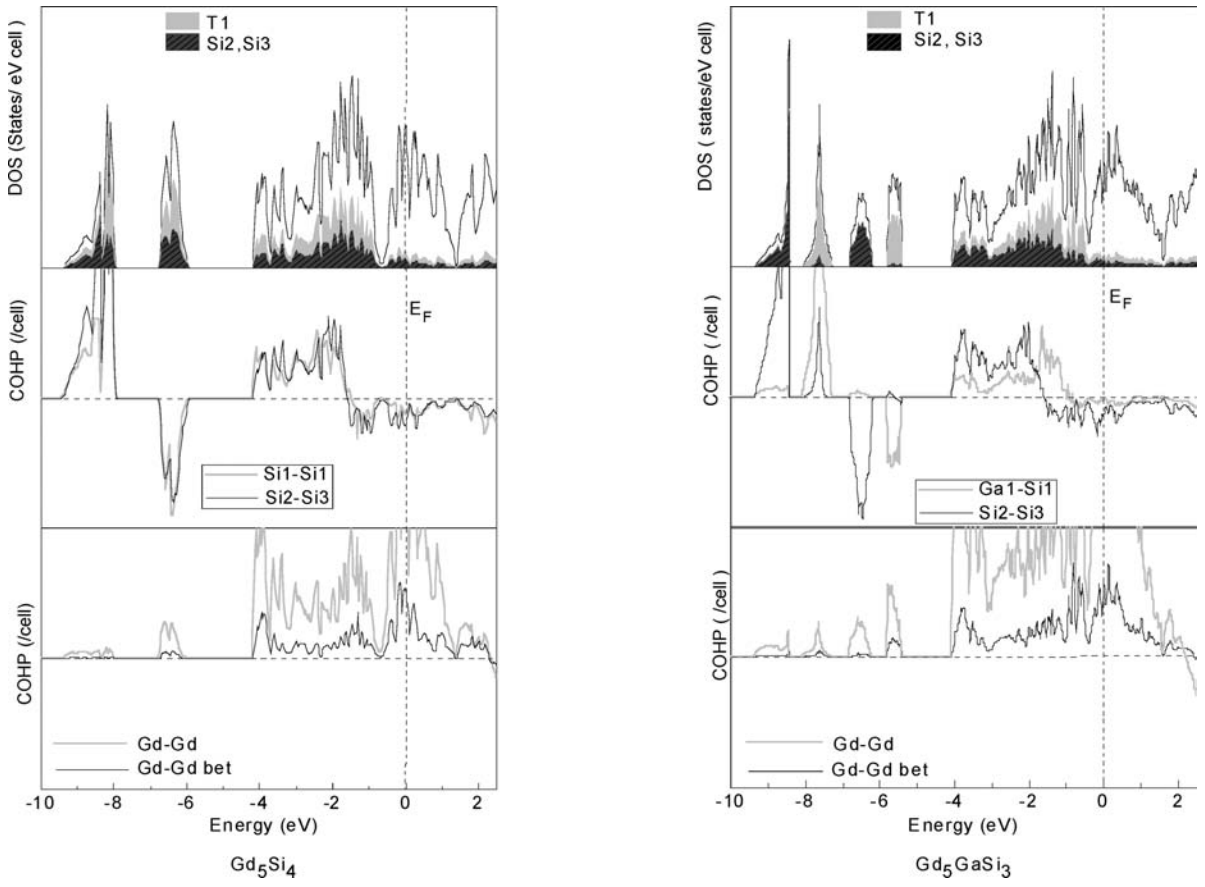

Figure 5. Total, projected DOS (top) and COHP curves for the T1-T1 and T2-T3 interactions (bottom) of Gd_5GaSi_3 and Gd_5Si_4. In Gd_5GaSi_3, Ga atoms are in the T1 site.

single crystal diffraction data for $Gd_5Ga_{0.99(4)}Si_{3.01}$ using the space groups for Models **A** and **C**, both of which are noncentrosymmetric. In both cases, we observed higher *R*-factors (0.043 and 0.047, respectively, for **A** and **C**) than for refinement in *Pnma* (0.0365) as well as similar, nonstatistical occupancies of Ga and Si atoms at all *T*-sites. Thus, entropy considerations play a significant role toward influencing the final site occupancies of the main group element (T) sites in $Gd_5(Ga_xSi_{1-x})_4$.

Density of States and Bonding Characteristics. Following the results of the energetic assessment of the coloring problem, DOS and COHP curves were calculated for the two end members of the $Gd_5Ga_xSi_{4-x}$ series identified in this investigation, that is, Gd_5Si_4 and Gd_5GaSi_3. As judged from the relative atomic arrangements and interatomic distances (see distances for Gd_5Si_4 and Gd_5GaSi_3 in Table 4 and previous discussion), structural perturbations introduced by Ga-doping are small, and are undoubtedly influenced by changes in both atomic sizes and valence electron count. The DOS and selected COHP plots for Gd_5Si_4 and the most stable model of Gd_5GaSi_3 (**A**) are presented in Figure 5 for comparison. The energy scales in both cases are presented with the corresponding Fermi levels as the reference (Gd_5Si_4: 31 valence electrons per formula unit; Gd_5GaSi_3: 30 valence electrons per formula unit).

The DOS curves for Gd_5Si_4 and Gd_5GaSi_3 have numerous common features, which arise from the fundamental Gd_5Si_4-type structure for both, but also show some important differences. The Fermi levels fall within bands that are largely Gd in character, bands dominated by Gd 5d with some 6s and 6p contributions. Below these calculated Fermi levels, both DOS curves reveal a pseudogap, which is more pronounced (deeper) for Gd_5Si_4 than Gd_5GaSi_3, corresponding to 28 valence electrons per formula unit for both cases. Below about −6 eV, T1−T1 and T2−T3 dimers are clearly evident by the bonding and antibonding σ_s and σ_s* levels: the electronegativity effect of Ga is seen by the presence of four bands in this region. Above about −4 eV, the DOS curves constitute a strong mixture of main group valence p orbitals with Gd 5d and 6s orbitals. Since the Fermi level for Gd_5GaSi_3 occurs for a lower valence electron count (30 e^-) than for Gd_5Si_4 (31 e^-), these valence bands have wider dispersion in the Ga-substituted case than in the binary silicide, although the unit cell volume is larger in Gd_5GaSi_3 than in Gd_5Si_4. Thus, there is favorable and greater orbital Gd−Ga orbital overlap than Gd−Si overlap.

Analysis of the COHP curves in Figure 5 provide some further insights into the structural tendencies and also provide a possible hint toward understanding the observed upper limit in Ga content in $Gd_5Ga_xSi_{4-x}$. As seen in many earlier studies,[11−13] T1−T1 and T2−T3 levels at the Fermi level in Gd_5Si_4 show antibonding character. The Si1−Si1 (2.493(6) Å) and Si2−Si3 (2.479(7) Å) distances are nearly equal, and the corresponding COHP curves are qualitatively similar; however, their integrated COHP values (2.593 eV for Si1−Si1 and 2.855 eV for Si2−Si3) indicate the Si1−Si1 contact to be intrinsically

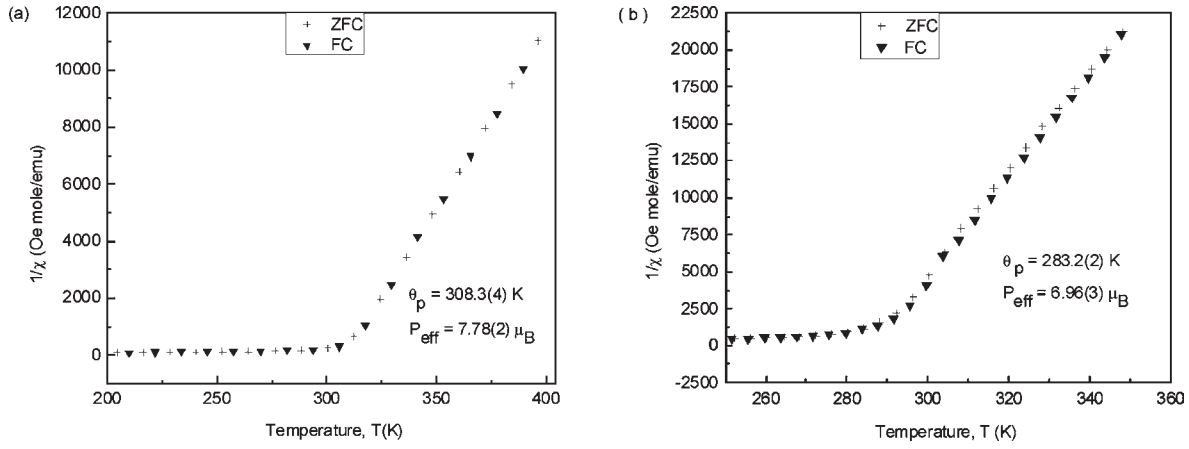

Figure 6. Inverse magnetic susceptibility plots for $Gd_5Ga_xSi_{4-x}$ (x = (a) 0.63, (b) 0.81).

weaker, that is, more susceptible to chemical substitution than the Si2−Si3 bond. This electronic effect derives from the different chemical environments of the two dimers: the Si1−Si1 bond has inversion symmetry (local symmetry is C_{2h}), while the Si2−Si3 has nearly D_{2h} symmetry.[13,35] Clearly, Si−Si π^* and σ^* antibonding states are occupied just below the Fermi level. In the corresponding Ga1−Si1 and Si2−Si3 COHP curves for Gd_5GaSi_3 (**A**) in Figure 5, two distinct differences from the Si−Si COHP curves in Gd_5Si_4 are evident: (1) Ga1−Si1 orbitals are very weakly antibonding (essentially nonbonding) around the Fermi level while the bonding/antibonding crossover occurs about 1.0 eV below the Fermi level; and (2) the occupation of Si2−Si3 antibonding orbitals is greater in Gd_5GaSi_3 than in Gd_5Si_4, although the valence electron count has decreased. Therefore, size and electronic effects counteract each other in subtle ways. With Ga substitution, Ga prefers the T-sites that have the weaker T−T interactions, but these also have higher volumes because they lie between slabs. The reduced valence electron count decreases occupation of T1−T1 π^* and σ^* antibonding states, so that the distance increment is smaller than may be anticipated. Finally, in Gd_5GaSi_3, the population of Si2−Si3 orbitals *increases* by about 0.5 electron because of the electronegativity effect on Ga1−Si1 orbitals. Thus, further substitution of Ga for Si may, in fact, increase the Si2−Si3 antibonding interaction, which can be a significant energetic driving force against further substitution and set the upper bound for $Gd_5Ga_xSi_{4-x}$.

Figure 5 also illustrates Gd−Gd COHP curves, and emphasizes interslab Gd−Gd contacts. These two sets of curves are quite similar in both Gd_5Si_4 and Gd_5GaSi_3 so that the lower valence electron count in Gd_5GaSi_3 reduces, overall, the strength of Gd−Gd interactions throughout the structure. Thus, Ga substitution provides both size and subtle electronic effects in the electronic DOS, effects which influence the observed compositions and the fine structural details.

Magnetometry. When Gd is combined with a nonmagnetic (semi)metallic element, the magnetic ordering temperature of the compound or alloy is nearly always lower than that of Gd (Gd, T_C = 294 K; Gd_5SiGe_3, T_C = 140 K; $Gd_5Si_2Ge_2$, T_C = 276 K; $GdAl_2$, T_C = 182 K). Therefore, it is very unusual that Gd_5Si_4, with 45 atomic percent nonmagnetic element Si, has a higher Curie temperature (T_C = 336 K) than that of pure Gd metal. Furthermore, magnetic measurements show that the temperature dependence of magnetization near T_C is much sharper than that predicted by molecular field theory (Brillouin function) for the Gd_5Si_4 compound.[36] Meanwhile, it was found that the T_C of Gd_5Si_4 could be lowered by substituting Ge for Si. Pecharsky et al. has studied the effect of many 3d- and p-element additions, substituting for nonmagnetic Si and Ge, on the magnetocaloric effect and found that Ga was the only one of all of those studied, such as Al, Fe, Co, Ni, Cu, and C, which increased the temperature of the first-order phase transition and simultaneously preserves a giant magnetocaloric effect. Thus, we began a quantitative and more extensive investigation of the influence of Ga on the Curie temperature of Gd_5Si_4. Figure 6 shows the results of magnetic susceptibility measurements in a 1 kOe field and the results of the numerical fitting for $Gd_5Ga_xSi_{4-x}$ (x = 0.63 and 0.81). The curves on heating (ZFC) and cooling cycles (FC) overlapped each other, and both show Curie−Weiss behavior at high temperatures. The effective paramagnetic moments, p_{eff}, were determined based on the numerical fitting for the data between 320 and 390 K and are shown in Figure 6. The effective moment for $Gd_5Ga_{0.63}Si_{3.37}$ is 7.78(2) μ_B, which is slightly lower than the free ion moment predicted for Gd^{3+} (7.94 μ_B), but the effective moment for $Gd_5Ga_{0.81}Si_{3.19}$ is 6.96(3) μ_B. The reason for this discrepancy is not well understood, while the results are reproducible for the same sample as well as for an independently prepared sample. Although this result could be ascribed to the existence of some unidentified noncrystalline minority phases, we have not verified this speculation.

The $M(H)$ plots are available in the Supporting Information; no obvious magnetic hysteresis could be detected in these two compounds. The Curie temperatures were estimated from dM/dT versus T plots to be, respectively, 310.3 and 286.3 K for $Gd_5Ga_{0.63}Si_{3.37}$ and $Gd_5Ga_{0.81}Si_{3.19}$. The paramagnetic Curie temperatures, θ_p, are shown in Figure 6, and are about 2−3 K lower than the corresponding Curie temperatures. The paramagnetic Curie temperature and Curie temperature decreased with increasing Ga

(35) Miller, G. J.; Lee, D.-S. Choe, W. *Highlights in Inorganic Chemistry*; Meyer, G., Naumann, D., Wesemann, L., Eds.; Wiley-VCH: Weinheim, Germany, 2002; p 21.

(36) Elbicki, J. M.; Zhang, L. Y.; Obermyer, R. T.; Wallace, W. E.; Sankar, S. G. *J. Appl. Phys.* **1991**, *69*, 5571.

content, which has the same trend of the substituting of Ge for Si. The effective paramagnetic moments for Gd ion in the two compounds are lower than the theoretical value (theoretical value for Gd^{3+}: 7.94 μ_B), and the reason is not well understood. But because the results are reproducible, it could probably be ascribed to the existence of some unidentified noncrystalline minority phases.

Conclusions

All $Gd_5Ga_xSi_{4-x}$ compounds crystallize in the orthorhombic Gd_5Si_4-type structure, space group *Pnma*. Single crystal refinements for the three crystallographic sites of Si/Ga atoms in the asymmetric unit reveal that Ga atoms prefer to occupy the interslab T1 sites over the intraslab T2 and T3 sites. The different behavior observed for the T1−T1 and T2−T3 distances along the $Gd_5Ga_xSi_{4-x}$ series is consistent with the systematically larger occupation of the larger Ga atom at the T1 site than in either the T2 or T3 sites. First principles calculations on different models of Gd_5GaSi_3 reveal having Ga atoms at the T1 sites results in the lowest electronic energy. Analysis of the COHP curves for the T−T contacts in Gd_5Si_4 indicates the Si1−Si1 bond to be intrinsically weaker and, therefore, more susceptible to chemical substitution, than the Si2−Si3 bond. With Ga substitution, Ga prefers the T1-sites, which have the weaker T−T interaction; meanwhile, the occupation of Si2−Si3 antibonding orbitals increases because of electronegativity effects. Therefore, increasing substitution of Ga for Si will enhance the Si2−Si3 antibonding interaction, an effect which can be a significant energetic driving force limiting the maximum Ga content and setting the upper bound for $Gd_5Ga_xSi_{4-x}$ near Gd_5GaSi_3. Magnetic susceptibility measurements of $Gd_5Ga_xSi_{4-x}$ (x = 0.63 and 0.81) show Curie−Weiss behavior at high temperatures as well as both Curie and Weiss temperatures decreasing with respect to those of Gd_5Si_4 with increasing Ga content, a trend which also occurs in $Gd_5Ge_xSi_{4-x}$.[10−12] The effective paramagnetic moments in the two compounds are lower than the theoretical value expected for Gd and the reason remains unclear at this point.

Acknowledgment. This manuscript has been authored by Iowa State University of Science and Technology under Contract No. DE-AC02-07CH11358 with the U.S. Department of Energy. The research was supported by the Office of the Basic Energy Sciences, Materials Sciences Division, U.S. DOE.

Supporting Information Available: Single crystal refinement data in CIF format, interatomic distances for $Gd_5Ga_{0.63}Si_{3.37}$ and $Gd_5Ga_{0.81}Si_{3.19}$; $M(H)$ plots for $Gd_5Ga_{0.63}Si_{3.37}$ and $Gd_5Ga_{0.81}Si_{3.19}$. This material is available free of charge via the Internet at http://pubs.acs.org.